Examining the event-shape-dependent modifications to charged-particle transverse momentum spectra and elliptic flow in *p*-Pb collisions at energies available at the CERN Large Hadron Collider

Somnath Kar,[1,2,*] Subikash Choudhury,[3,†] Xiaoming Zhang,[1,‡] and Daicui Zhou[1,§]

[1]*Key Laboratory of Quark and Lepton Physics (MoE) and Institute of Particle Physics, Central China Normal University, Wuhan 430079, China*

[2]*Nuclear and Particle Physics Research Centre, Department of Physics, Jadavpur University, Kolkata - 700032, India*

[3]*Key Laboratory of Nuclear Physics and Ion-beam Application (MoE) and Institute of Modern Physics, Fudan University, Shanghai 200433, China*

(Received 4 January 2020; revised 23 July 2020; accepted 27 August 2020; published 1 October 2020)

Purported signatures of collective dynamics in small systems like proton-proton (pp) or proton-nucleus (p-A) collisions still lack unambiguous understanding. Despite the qualitative and/or quantitative agreement of the data to hydrodynamic models, it has remained unclear whether the harmonic flows in small systems relate to the common physical picture of hydrodynamic collectivity driven by the initial geometry. In the present work, we aim to address this issue by invoking a novel concept of event shape engineering (ESE), which has been leveraged to get some control of the initial geometry in high-energy heavy-ion collisions. We utilize ESE by constructing a reference flow vector, q_2 that allows to characterize an event based on its ellipticity. Applying this technique on a data set, simulated from a 3 + 1 dimensional viscous hydrodynamic model EPOS3, we study the event-shape dependent modifications to some of the bulk properties, such as inclusive transverse momentum (p_T) spectra and p_T-differential v_2 for p-Pb collisions at 5.02 TeV. Selecting events on the basis of different magnitudes of reference flow vector q_2, we observe a hint of event-shape induced modifications of v_2 as a function of p_T, but the inclusive p_T spectra of charged particles seem to be insensitive to this event-shape selection.

DOI: 10.1103/PhysRevC.102.044901

I. INTRODUCTION

Hydrodynamic modeling has remained the most successful description to the properties of the bulk matter produced in the collisions of heavy nuclei at ultrarelativistic energies [1,2]. The efficacy of hydrodynamic calculations have not only allowed to characterize the medium produced in these collisions as a strongly interacting fluid, but, also, presented unambiguous evidences that relate final state momentum space azimuthal anisotropies to the spatial inhomogeneities in the initial stage. It is generally perceived that an inviscid hydrodynamic evolution efficiently translates these initial inhomogeneities in the initial state to the final state momentum space azimuthal anisotropies—quantified by the coefficients v_ns in the Fourier decomposition of the azimuthal distributions of produced particles in a plane transverse to the beam axis [3–5].

For a long time, the applicability of the hydrodynamic models were thought to be limited to large and extended systems like the one produced in heavy-ion collisions. However, only recently, it was realized that the dynamical behavior of the medium produced in hadron-hadron or hadron-on-ion collisions (small systems) exhibit remarkable similarity to those of the heavy-ions [6–9]. Notably, the agreement of hydrodynamic calculation to unexpectedly large values of anisotropic flow coefficients triggered speculations of whether the collisions of small systems are also dominated by strong final state interactions. [10,11]. However, it must be mentioned that the strongly interacting nature of the medium produced in large systems were not only inferred from the agreement of hydrodynamic calculations to the measurements of p_{T}-differential yields and anisotropic flow coefficients at low-p_{T}, but, also, corroborated by the concurrent observations of the energy loss of high-p_{T} particles/jets which by far remain elusive in small systems [12–14]. In addition, the so-called hallmark of the hydrodynamic collectivity, in particular, the sizable magnitudes of flow harmonics in small systems are also confronted by distinctly different suite of physical interpretations where strong final state interactions have not been invoked [15–19]. This counterintuitive observation of the hydro-like collectivity, in the absence of the jet-quenching, therefore, underscores the importance of studying the emergent phenomenon of collective dynamics in small systems with all forms of available tools at our disposal.

*somnathkar11@gmail.com
†subikash@fudan.edu.cn
‡xiaoming.zhang@mail.ccnu.edu.cn
§dczhou@mail.ccnu.edu.cn

Recently, a test of hydrodynamization in small systems was conducted at the BNL Relativistic Heavy Ion Collider (RHIC) with shape engineered collision species; p-Au, d-Au, and He-Au collisions, producing intrinsically circular, elliptic, and triangular configurations, respectively, in their initial geometry [20]. It was argued that the imprints of this initial geometry will be reflected at the final stage provided the hydrodynamic collectivity prevails. For example, if the system has an intrinsic elliptic or triangular shape, hydrodynamic collectivity would favor an ordering between the final state elliptic (v_2) and triangular (v_3) flow coefficients [11,21]. The measurements of $v_{2,3}$ by the PHENIX collaboration indeed presented some evidence in favor of this conjectured correlations between the initial geometry and hydroexpected ordering in the flow patterns [20]. Therefore, further experimental investigations on such initial geometry dependent ordering of harmonic flows at higher $\sqrt{s}$ might be timely and desirable to corroborate the claims of common hydrodynamic paradigm across widely different system sizes [22]. However, to date, the scopes of exploring the fluid dynamical picture in small systems with intrinsically different initial geometries at the CERN Large Hadron Collider (LHC) energies are unlikely. Notwithstanding this limitation, the influence of initial geometry on the final state momentum space anisotropy of the produced particles can therefore be examined with an alternative novel technique namely, the event shape engineering (ESE) [23].

In the framework of Glauber-like initial condition followed by the hydrodynamic evolution, the event-by-event fluctuations in the distributions of the initial nuclear matter is manifested as a large spread in the distributions of initial and final state anisotropies [24]. This can be eventually exploited to further categorize events into different classes of initial geometry but at comparable multiplicity. This technique of selecting events on the basis of initial geometry is generally referred to as the event shape engineering. A key component of this technique is the determination of reference flow vectors q_ns ($n = 2$, 3, etc.) in the momentum space, which by construction are correlated to nth order harmonic (for $n < 4$) flow coefficients and hence to the corresponding orders of asymmetries at the initial co-ordinate space [25]. Here, it must be mentioned, unlike the hydrodynamic descriptions that relate the flow harmonics to the initial geometry, the flow-like signals in the color glass condensate (CGC) effective field theory (EFT), on the other hand, are attributed to initial state gluon momentum correlations which depend on a saturation length scale ($1/Q_s$) via event multiplicity. Therefore, the flow harmonics within the CGC theory are supposedly independent of the event geometry. As a result, the ESE technique could be used as an effective tool to distinguish the underlying origin of harmonic flows in small systems.

Since the original proposal, the ESE technique has been applied to several experimental measurements either to constrain the flow-induced backgrounds or to investigate the degree of correlations between different orders of flow harmonics [26–28]. In this work, we examine the response of the bulk properties of the produced medium at the final state to the variations in the magnitudes of the initial spatial asymmetries by applying the ESE technique to a small system such as p-Pb collisions at 5.02 TeV. Using an event-by-event $3 + 1$-dimensional ($3 + 1$D) viscous hydrodynamic model, EPOS3, we investigate the modifications to the inclusive yields and the elliptic flow coefficient, v_2 of charged particles as a function of p_T, for an ensemble of events with higher or lower than the average bulk elliptic flow anisotropy, quantified by the reduced second order flow-vector, q_2.

The remainder of this paper is structured as follows. In Sec. II we provide a brief account of the hydrodynamic model EPOS3, followed by the analysis details in Sec. III. In Sec. IV we present the results and finally we discuss and summarize in Sec. V.

II. EPOS3: THE MODEL

EPOS3 is built on a pQCD inspired framework for Gribov-Regge multiple parton scattering approach, where an individual scattering generates a longitudinally stretched colored flux tube (strings) with transverse kinks carrying p_T from the initial hard scatterings [29]. These flux tubes eventually break into pairs of string segments that lead to the production of final state particles following Schwinger mechanism of string fragmentation.

A high multiplicity event in EPOS3 is characterized by a highly dense medium of colored strings produced from a large number of parton-parton interactions. Under such conditions, several strings overlap each other which prevent them from hadronizing independently, as described above. In this situation, EPOS3 classifies these strings to constitute either jets or the bulk matter. Based on an energy loss formalism, fate of the strings are decided, i.e., whether they will be a part of the bulk matter or emerge out as high-p_T particles/jets [30]. If the fractional energy loss of string segments exceed a certain threshold which is a model dependent parameter, they constitute the bulk matter, the so-called core, that undergo a viscous hydrodynamic expansion and hadronize by the usual Cooper-Frye formalism at a hadronization temperature, T_H. The rest of the string segments form a corona and hadronize by the usual Schwinger mechanism. In general, EPOS3 is able to describe some aspects of the data in small collision systems reasonably well. This includes the double-ridge structure in the two-particle angular correlations, the p_T dependence and the characteristic mass ordering of v_2, among others [31,32].

To verify, whether the simulated EPOS3 event samples can emulate some aspects of the p-Pb data, we calculate $v_2(p_T)$ of pions and protons for 0–20% most central p-Pb events and compare the same with published ALICE results [33] in Fig. 1. In one of our previous publications [30], we also compared the multiplicity dependent invariant yields of identified particles as a function p_T calculated from the EPOS3-generated events to the data. In both cases agreement with the data are well founded. Having observed a good agreement between data and simulated events, we proceed further to testify the central theme of our present work.

III. ANALYSIS

A. Centrality and the event-shape (q_2) determination

EPOS3 generated event samples are first subsampled into multiplicity (centrality) classes based on the particle

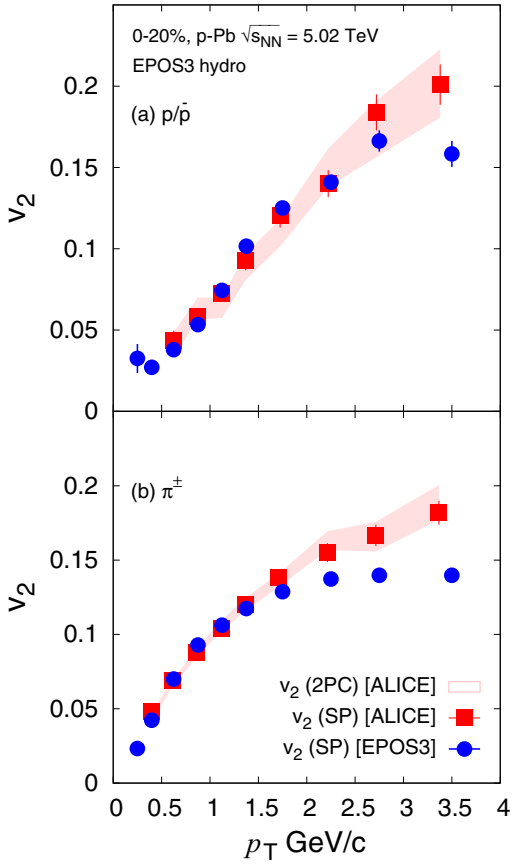

FIG. 1. Elliptic flow parameter v_2 for (a) protons ($p + \bar{p}$) and (b) pions ($\pi^+ + \pi^-$) as a function of p_T calculated from full hydrodynamic simulation of EPOS3 for 0–20% most central p-Pb events at $\sqrt{s_{NN}} = 5.02$ TeV.

multiplicity in the pseudorapidity coverage, $2.8 < \eta < 5.1$, corresponding to ALICE V0A detector acceptance [34]. Details of the centrality selection from the minimum bias EPOS3 generated p-Pb samples can be found here [30].

In a given multiplicity interval, these events are further categorized into different classes of reduced second-order harmonic flow vector, q_2 defined as [25,35]

$$q_2 = |Q_2|/\sqrt{M}, \tag{1}$$

where M corresponds to number of particles used in the calculation of the second-order harmonic flow vector, Q_2. The definition for the flow vector Q_2 is

$$|Q_2| = \sqrt{Q_{2x}^2 + Q_{2y}^2}, \tag{2}$$

where Q_{2x}, Q_{2y} correspond to the cosine and sine component of flow vector Q_2, respectively.

In this work, we calculate q_2 in the p_T-range $0.2 < p_T < 20$ GeV/c at two different pseudorapidity regions; one in the midrapidity, $|\eta| < 0.3$ and others in the forward rapidity, $-1.7 < \eta < -3.7$. The former has an overlap with the detector coverage of ALICE-TPC [36] while, the latter is equivalent to ALICE-V0C [37] acceptance. Hereafter in the text and in figures, we will refer q_2 calculated in these two regions as

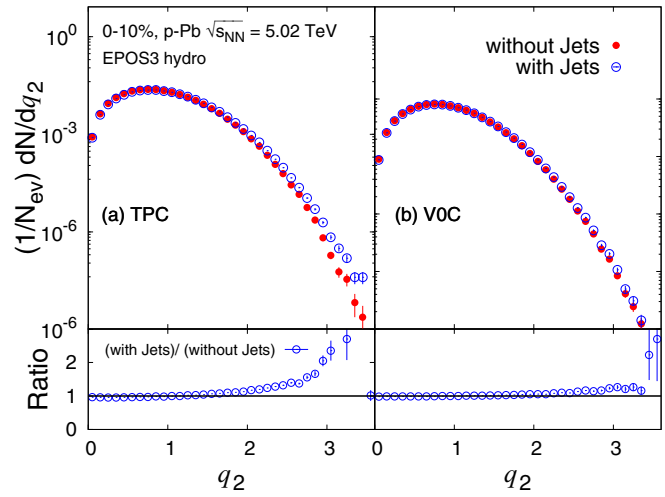

FIG. 2. Distributions of second order reference flow vector q_2 calculated in the equivalent η acceptance of (a) ALICE-TPC and (b) ALICE-V0C with and without subtractions of jetty events. The lower panels show the ratio of q_2 distributions with and without subtraction of jetty events for both $q_2^{\rm TPC}$ and $q_2^{\rm V0C}$.

$q_2^{\rm TPC}$ and $q_2^{\rm V0C}$, respectively. Figure 2 shows the $q_2^{\rm TPC}$ ($q_2^{\rm V0C}$) distributions for 0–10% highest multiplicity events.

As the particle production in small systems is dominated by the pQCD processes, flow vectors so obtained are presumably vulnerable to large nonflow effect from dijets, diminijets, and also resonance decays. In general, the contributions from the nonflow effects scale inversely with particle multiplicity M, where M could be the number of particles used in the determination of flow vector, Q_2. Therefore, we will mostly focus on the high-multiplicity events rendering an automatic reduction to the nonflow effects. Although, such a choice can naturally reduce the nonflow contributions in larger systems where particle multiplicity is originally high but this may not be strictly true for small systems where the overall particle multiplicity is less. Thus, to further mitigate the nonflow related contributions to q_2 we invoke rejection of events that has a jet of minimum jet-p_T (without background subtraction) of 5 GeV/c. To do so we make use of the jet reconstruction technique where jets are reconstructed using the standard anti-k_T jet-finding algorithm in the FASTJET package [38] for resolution parameter $R = 0.2$.

The effect of removing jetty events can be readily observed from the ratios of $q_2^{\rm TPC}$ distributions, before and after the removal of jetty events in Fig. 2. Towards the higher values of $q_2^{\rm TPC}$, ratios differ from unity by 50% or more, implying a substantial jet bias. But the difference is less prominent for $q_2^{\rm V0C}$, suggestive of its robustness against jet contamination. However, the observed effect for $q_2^{\rm V0C}$ may be completely model dependent. A possible reason that we can think of is the drop in dijet or diminijet yields in EPOS3, away from the midrapidity. However, $q_2^{\rm V0C}$ has an advantage over $q_2^{\rm TPC}$ as it provides a large natural pseudorapidity ($|\Delta\eta|$) separation between regions of calculated Q vectors and the observables of physics interest (which is calculated here within $0.5 < |\eta| < 1$). This is rather crucial for the removal of the

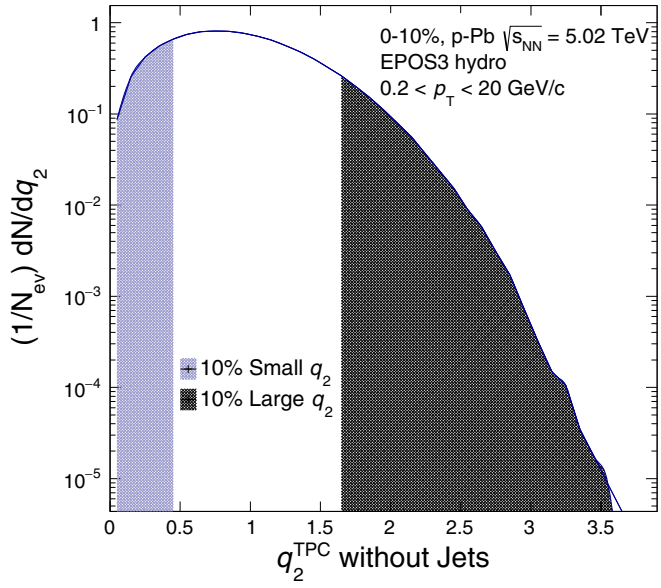

FIG. 3. Representations of 10%-large (small) selection areas in the q_2 distribution calculated in the TPC region after the removal of jetty events.

autocorrelations and the correlated nonflow effects. But, for $q_2^{\rm TPC}$, we could only afford a maximum $|\Delta\eta|$ gap of 0.2 unit, because of our choice of limited η coverage of ± 1, to be able to comply with ALICE-TPC acceptance.

Figure 3 shows the jet subtracted $q_2^{\rm TPC}$ distribution for 0–10% highest multiplicity events and the shaded regions in the same correspond to the top and bottom 10% of events with highest and lowest values of $q_2^{\rm TPC}$, respectively. We will calculate the physics observables in this highest (0–10%) and lowest (90–100%) 10% bins of $q_2^{\rm TPC}$ as well as $q_2^{\rm V0C}$, which will be referred to in the remainder of the text as large and small $q_2^{\rm TPC}$or $q_2^{\rm V0C}$, respectively. To be mentioned, because of limited statistics, we report our results averaged over an interval of 10% multiplicity bin, but the ESE-selection classes are defined based on q_2 percentiles obtained from 1% multiplicity bin width in order to avoid any trivial fluctuations in q_2 due to fluctuations in the particle multiplicity.

IV. RESULTS

A. Transverse momentum distributions

Effect of event-shape selection is first studied on the single inclusive charged particle $p_{\rm T}$ spectra for large and small-$q_2^{\rm TPC}$ and $q_2^{\rm V0C}$ event samples and reported in Fig. 4. As mentioned, to avoid overlap with the η range of $q_2^{\rm TPC}$ ($|\eta| < 0.3$), the $p_{\rm T}$ distributions of unidentified charged particles are calculated in the range $0.5 < |\eta| < 1.0$. In order to study how the jet contamination in q_2 affects the event-shape selections and hence the modifications of $p_{\rm T}$ spectra in shape-engineered event samples, we calculate the ratios of charged particle $p_{\rm T}$ spectra in shape-biased to shape-unbiased events on the basis of 10% highest and lowest q_2 percentiles, derived from q_2 distributions with and without jet contaminations as shown in Fig. 2. Blue and red bands in Fig. 4 correspond to the results obtained from event-shape selection based on the q_2 distributions including jet bias. On the other hand, markers in Fig. 4 represent the same results except the q_2 percentiles are determined from q_2 distributions without jet bias. The effect of jet contamination in q_2 is manifestly evident from the comparison of these two cases. When the q_2 percentiles are extracted from the q_2 distributions including jetty events,

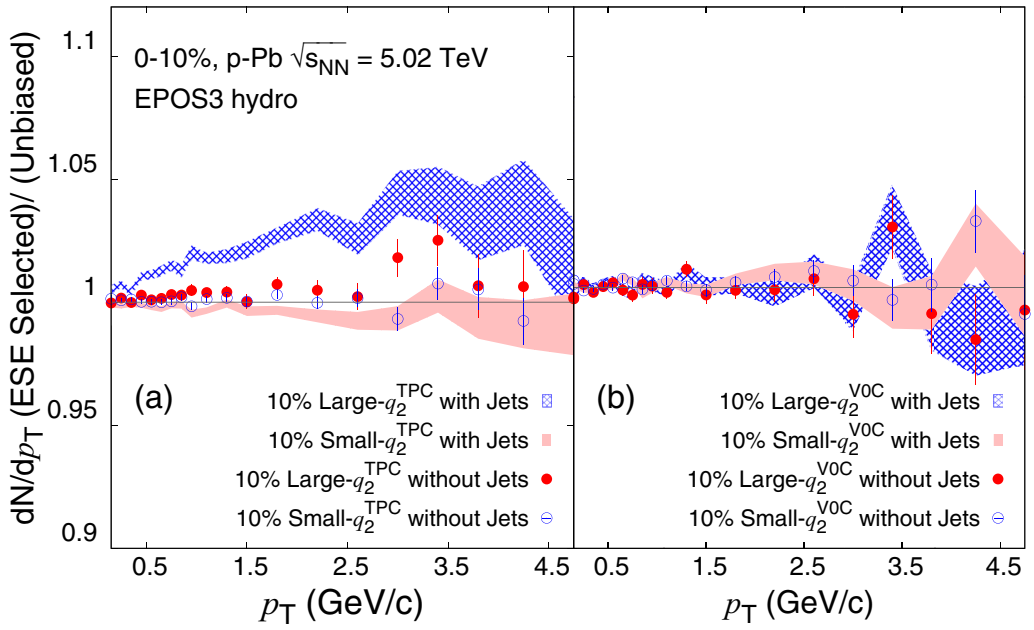

FIG. 4. Ratio of charge particle yields in ESE-selected events with respect to unbiased sample as a function of transverse momentum for (a) $q_2^{\rm TPC}$ and (b) $q_2^{\rm V0C}$ for the EPOS3 simulated events with hydro in p-Pb collisions at $\sqrt{s_{NN}} = 5.02$ TeV. A comparison of with and without removal of jetty events is also shown for both the regions of q_2 selections.

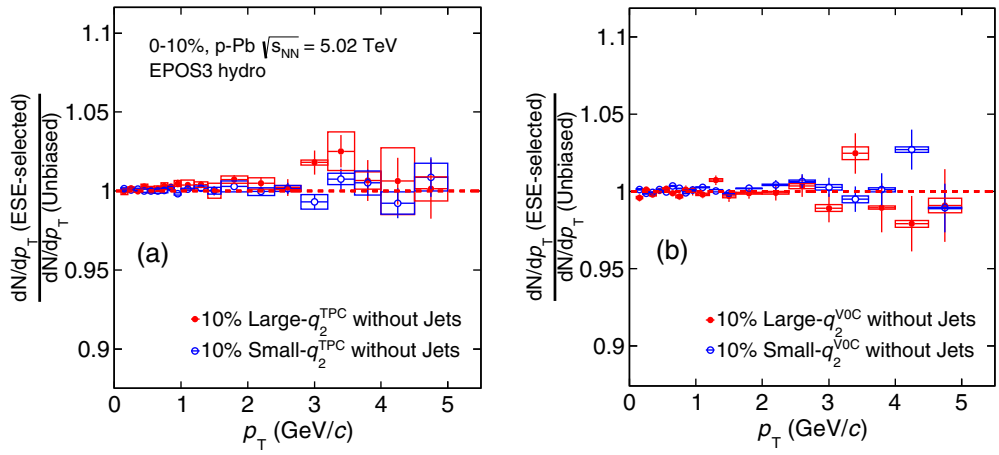

FIG. 5. Systematic variations of ratio of charge particle yields as a function of transverse momentum in ESE-selected events with respect to unbiased sample after the removal of jetty events for (a) q_2^{TPC} and (b) q_2^{V0C}.

ratios of p_{T} spectra in shape-biased to unbiased event samples exhibit an increasing trend with increasing p_{T}. However, upon removal of the jetty events and recalculating the q_2 percentiles based on the q_2 distribution without jet contamination, the ratio is rather flat and consistent with unity. This suggests that the apparent hardening of the spectral shape, in particular, in large-q_2 events could be because the mean of the q_2 distribution is shifted towards the higher values due to systematic bias from the jet-dominated events.

Also for q_2^{V0C} selection, the aforementioned exercise is repeated to study the possible modifications to the spectral shape in large and small-q_2^{V0C} event samples relative to the shape-unbiased sample. In a marked contrast to q_2^{TPC}, shape selection on the basis q_2^{V0C} is seemingly unaffected by the jet contamination. This agrees with our previous observation in Fig. 2, where the impact of the removal of jetty events was found to be insignificant on q_2^{V0C} distributions itself.

As we observed that the removal of jetty events has a large impact on the shape dependent charge particle yields, we therefore proceeded to do some systematic checks to establish the robustness of these results. Since, we consider only reconstructed jet-p_{T} without background subtraction, there could be chances of an overestimation of jet-p_{T} resulting in the removal of events in excess to what is needed. Therefore, to understand whether our final results are stable against this proposed jetty event removal technique, we repeated the analysis varying the minimum p_{T} of the input particles that are fed into the jet-reconstruction algorithm.

The minimum p_{T} of input particles taken so far as a default choice is 0.3 GeV/c. For systematics, this value is changed to 0.15 and 0.5 GeV/c, respectively. Subsequently, jets are reconstructed with the corresponding sets of input particles, followed by the removal of jetty events from the q_2 distribution in the same way as previously mentioned. The open boxes in Fig. 5 represent the systematic variation on the ratios plotted in Fig. 4 and indicated by solid and open markers. The systematic changes in the ratio are well within the limits of current statistical uncertainties.

B. Elliptic flow

In this section we report the results of the elliptic flow coefficient of charged particles in unbiased and shaped-engineered event samples. The elliptic flow coefficient, v_2, as a function of p_{T} is calculated in the pseudorapidity range $0.5 < |\eta| < 1.0$, using the scalar product method [39,40]. In this method, an event is divided into subevents without an overlap in pseudorapidity. This is done by defining at least two subevents separated by an η gap. Here, we have defined two subevents A and B covering the η range $-0.5 < \eta < -1.0$ and $0.5 < \eta < 1.0$, respectively, and calculated $v_2(p_{\mathrm{T}})$ according to the relation

$$v_2\{SP\}(p_T) = \frac{\langle u_{2,i} Q_2^*/M \rangle}{\sqrt{\langle Q_{2,A} Q_{2,B}^*/M_A M_B \rangle}}, \tag{3}$$

where $u_{2,\mathrm{i}} = e^{2\phi_i}$ is the unit vector of the ith particle of interest, ϕ_i is the corresponding azimuthal angle, and Q_2^*/M is the multiplicity normalized second order flow vector. In the denominator, $Q_{2,\mathrm{A}}$ (M_{A}) and $Q_{2,\mathrm{B}}$ (M_{B}) are the second-order flow vectors (multiplicity) in subevents A and B, respectively. The angular bracket in the numerator indicates the average over all particles of interest. To suppress nonflow contributions to v_2, the unit flow vector $u_{2,\mathrm{i}}$ and the flow vector Q_2 are always evaluated from different subevents.

Figure 6 shows the correlation between the p_{T}-average elliptic flow coefficient, $\langle v_2 \rangle$, and q_2 for q_2^{TPC} [Fig. 6(a)] and q_2^{V0C} [Fig. 6(b)]. The q_2 values are calculated under two conditions: with (blue) and without (red) jet contribution. The $\langle v_2 \rangle$ exhibits a slight increasing trend for both q_2^{TPC} and q_2^{V0C}, but the increase is rather sharp for $q_2^{\mathrm{TPC}} > 2$. This could be due to some correlated residual nonflow effect as the $|\eta|$ gap available for q_2^{TPC} is small.

Figure 7 shows v_2 as a function of p_{T} in large, small, and unbiased-q_2 event samples after the subtraction of jetty events from both q_2^{TPC} and q_2^{V0C}. The top row of Fig. 7 shows the charged particle $v_2(p_{\mathrm{T}})$ in large and small-q_2^{TPC} event samples [Fig. 7(a)] and the ratios of $v_2(p_{\mathrm{T}})$ [Fig. 7(b)] in large and

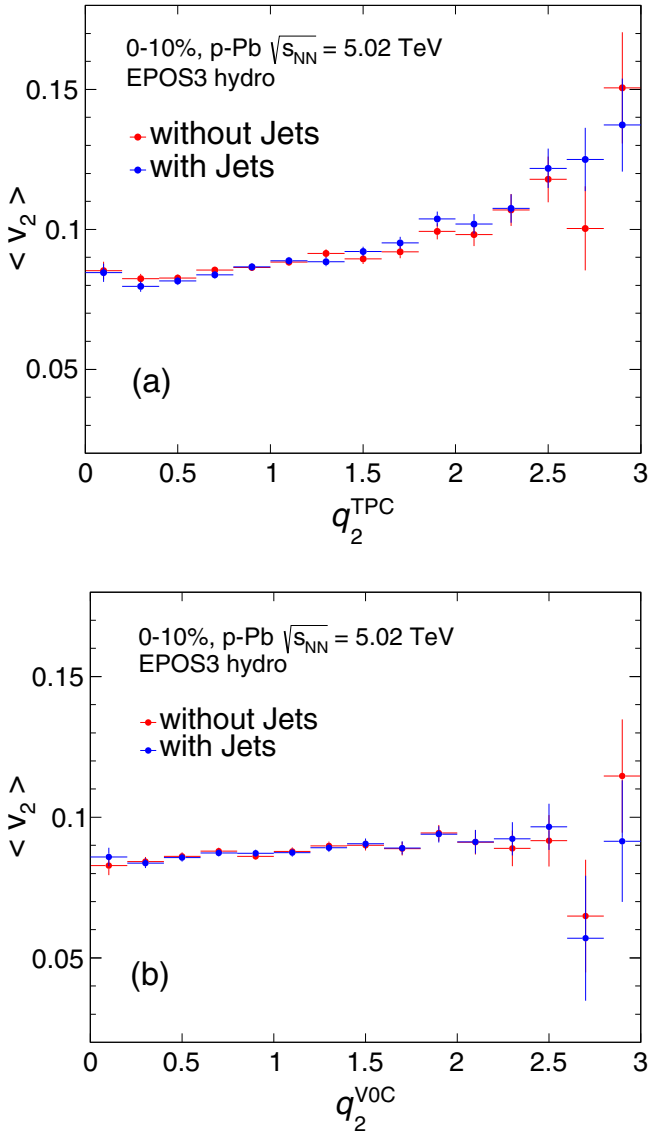

FIG. 6. Correlations between average elliptic flow coefficient v_2 and q_2 measured in (a) TPC and (b) V0C regions for unidentified charged particles, with and without removal of jetty events from $q_2^{\rm TPC}$ and $q_2^{\rm V0C}$.

small-$q_2^{\rm TPC}$ event samples relative to the shape-inclusive one for the event-shape selection based on $q_2^{\rm TPC}$. The same for $q_2^{\rm V0C}$ are shown in the bottom panel [Fig. 7(c) and 7(d)]. It can be observed that for 10% large (small)-$q_2^{\rm TPC}$ selection, $v_2(p_{\rm T})$ changes by 20% (10%) with no significant $p_{\rm T}$ dependence. In contrary, no noticeable difference is observed when the event-shape selection is based on $q_2^{\rm V0C}$. We also repeat the same systematic study for $v_2(p_{\rm T})$, as it was done for $p_{\rm T}$-differential yields in the previous section.

V. DISCUSSIONS AND SUMMARY

The role of initial geometry as an essential ingredient to the dynamics of multiparticle angular correlations in relativistic heavy-ion collisions has been established in light of hydrodynamic calculations that predict strong linear correlations between coefficients of final state azimuthal anisotropy (v_n, $n < 3$) and the corresponding initial spatial asymmetry (ϵ_2, ϵ_3). Of late, studies on small collision systems have also presented evidence that are typical of the standard picture of the hydrodynamic evolution in heavy-ion collisions. Although the generalization of hydrodynamic calculations to small systems has become a standard practice nonetheless, its applicability has remained highly debated. In view of this existing ambiguity on the issue whether the observed features of azimuthal correlations in small systems are consequences of strong final state interactions resulting in hydrodynamic evolution or manifestations of other physical processes related to the initial state gluon correlations, we employ ESE as a tool to probe the degree of correlation between initial geometrical inhomogeneity and final state azimuthal anisotropy. Making use of the ESE technique we study modifications to the charged particle transverse momentum spectra and elliptic flow coefficients in shape engineered in 0–10% central p-Pb events at 5.02 TeV using a 3 + 1D viscous hydrodynamic model, EPOS3.

Events are first categorized according to the magnitudes of q_2 vector calculated at different $|\eta|$ acceptances referred to as $q_2^{\rm TPC}$ and $q_2^{\rm V0C}$. As the determination of q_2 vectors in small systems are susceptible to nonflow effects from dijets and diminijets, we eliminate events with jet-$p_{\rm T} > 5$ GeV/c. The effect of removing jetty events can be immediately observed from Fig. 2. At large values of q_2 (>2) a surge in the ratio of q_2 distribution with and without the removal of jetty events can be noticed. This could be due to the fact that very large values of q_2 arise from the events dominated by jet-like processes.

The ratio of $p_{\rm T}$-differential yields of charged particle spectra in ESE-selected events to those unbiased events shown in Fig. 4 exhibits hardening (softening) in large-$q_2^{\rm TPC}$ (small-$q_2^{\rm TPC}$) samples when classification was done on the basis $q_2^{\rm TPC}$ calculated without removing jetty events. On the removal of jet contamination and reclassification of large- and small-$q_2^{\rm TPC}$ event samples, no significant difference in the ratios of $p_{\rm T}$-differential yields are observed for $q_2^{\rm TPC}$ event-shape selection rather the ratios of yields in shape biased to unbiased event samples are seen to be consistent with unity. This confirms that q_2 distributions in small systems, in particular, have large nonflow bias. A similar calculation repeated on the basis of $q_2^{\rm V0C}$ is also consistent with unity and shows no effect of jet subtraction.

At this point we recollect that the measurements of event-shape dependent modifications to $p_{\rm T}$ spectra in heavy-ion collisions by ALICE [25] revealed that the $p_{\rm T}$ spectra in large and small q_2 events exhibit significant hardening and softening respectively. This has been attributed to the correlation between the event eccentricity and the radial boost, i.e., events with larger eccentricity have increased radial push. But with a full hydrodynamic simulation of a small system, like the one studied here, we find no such evidence of a correlation between eccentricity and radial boost. This may be because the initial energy deposition profile in small systems is so smeared that the average energy-density and initial eccentricity is either uncorrelated or weakly correlated. We substantiate on this assertion by extracting kinetic freezeout temperature $T_{\rm kin}$ and

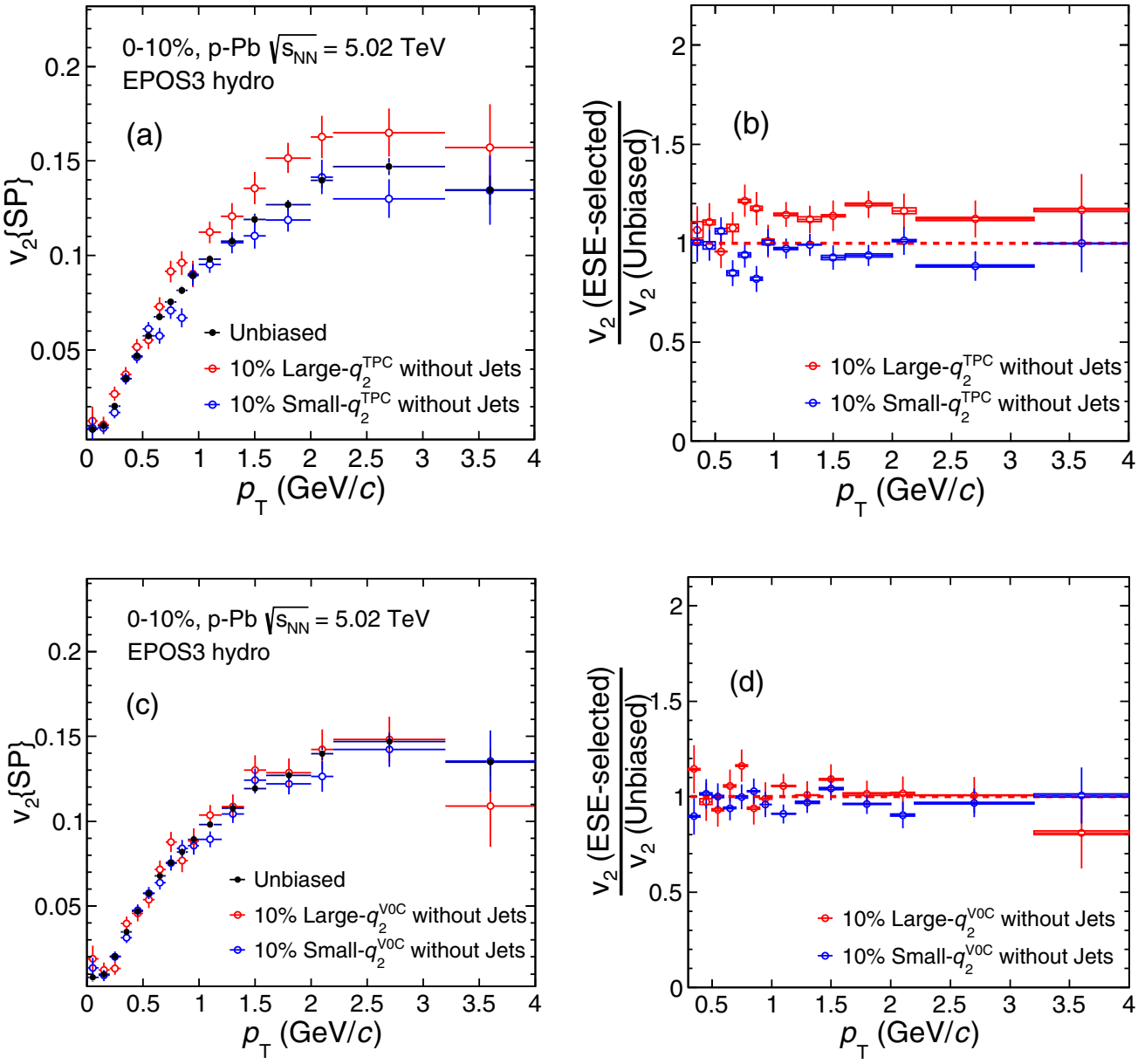

FIG. 7. Elliptic flow coefficient v_2 as a function of p_T in ESE-selected and unbiased event samples and the ratio of ESE-selected event samples to the unbiased one for q_2^{TPC} (a, b) and q_2^{V0C} (c, d) after the removal of jetty events. The systematic variations to the ratios of v_2 for the ESE-selected event samples to the unbiased sample are shown with open boxes which are however too small to see with naked eyes.

radial boost parameter β in large and small-q_2 event samples via a simultaneous blast-wave fit [41] to pion, kaon, and proton p_T spectra. The values obtained, tabulated in Table I, suggest that in the collisions of small systems, radial boost or freezeout temperature are either independent or insensitive to the initial event geometry.

TABLE I. Parameters for bast-wave fit.

	Temperature (T_{kin}) in GeV	β
Large-q_2	0.114	0.534
Small-q_2	0.115	0.531

Furthermore, we investigate the effect event-shape engineering on both p_T-differential and p_T-integrated elliptic flow coefficients, v_2 at midrapidity. Figure 6 shows an increasing trend in p_T-average v_2 for both q_2^{TPC} and q_2^{V0C} but the increase is more prominent for q_2^{TPC} than q_2^{V0C}. This is most likely because of the reduced sensitivity of q_2^{V0C} to the global event-shape together with the longitudinal decorrelation effect which is expected to be large in asymmetric small collision systems. Whereas, for q_2^{TPC}, we do observe a relatively sharp rising trend of $\langle v_2 \rangle$ but we cannot completely ignore correlated nonflow effects as the available η gap is much less. Similar arguments are also valid for p_T-differential v_2 (shown in Fig. 7) which shows the sensitivity of event-shape selection largely depends on the choice of q_2 vector.

To summarize, in this article we make an attempt to assess, whether the final state momentum space anisotropies in small systems originate from correlations limited to a few particles or can be linked to global event properties, those associated with event shapes or profile. In addition, we also realize that the variable used to gauge the event shape, i.e., q_2, is very much affected by nonflow components mostly stemming from dijets and diminijets. Therefore, we adopt a scheme to minimize nonflow effects by discarding events dominated by jets. Within the current level of uncertainties we observe the event-shape dependent modifications of v_2 are in line with ESE expectations provided the reference flow vector (q_2) and particles of interest are not widely separated in η.

Experimental verification of this new set of results is certainly warranted in order to advance our understandings of the initial conditions and the subsequent spatiotemporal evolutions in so-called small collision systems at relativistic energies.

ACKNOWLEDGMENTS

The authors are thankful to Dr. Klaus Werner for providing them with the EPOS3 code and related discussions. This work is supported by the National Natural Science Foundation of China (Grants No. 11805079 and No. 11775097), national key research and development program (Grants No. 2018YFE0104700, No. 2015CB856905), and No. CCNU18ZDPY04. One of the authors (S.K.) acknowledges the financial support from UGC-INDIA Dr. D. S. Kothari Post Doctoral Fellowship under Grant No. F.4-2/2006(BSR)/PH/19-20/0039.

[1] U. W. Heinz and R. Snellings, Annu. Rev. Nucl. Part. Sci. **63**, 123 (2013).
[2] P. Romatschke and U. Romatschke, in *Relativistic Fluid Dynamics In and Out of Equilibrium*, Cambridge Monographs on Mathematical Physics (Cambridge University Press, Cambridge, 2019).
[3] B. Schenke, S. Jeon, and C. Gale, Phys. Rev. Lett. **106**, 042301 (2011).
[4] B. Schenke, S. Jeon, and C. Gale, Phys. Rev. C **85**, 024901 (2012).
[5] A. M. Poskanzer and S. A. Voloshin, Phys. Rev. C **58**, 1671 (1998).
[6] S. Chatrchyan *et al.* (CMS Collaboration), Phys. Lett. B **718**, 795 (2013).
[7] B. Abelev *et al.* (ALICE Collaboration), Phys. Lett. B **719**, 29 (2013).
[8] G. Aad *et al.* (ATLAS Collaboration), Phys. Rev. Lett. **110**, 182302 (2013).
[9] A. Adare *et al.* (PHENIX Collaboration), Phys. Rev. Lett. **111**, 212301 (2013).
[10] K. Werner, M. Bleicher, B. Guiot, Iu. Karpenko, and T. Pierog, Phys. Rev. Lett. **112**, 232301 (2014).
[11] J. L. Nagle, A. Adare, S. Beckman, T. Koblesky, J. Orjuela Koop, D. McGlinchey, P. Romatschke, J. Carlson, J. E. Lynn, and M. McCumber, Phys. Rev. Lett. **113**, 112301 (2014).
[12] J. Adam *et al.* (ALICE Collaboration), Phys. Lett. B **760**, 720 (2016).
[13] V. Khachatryan *et al.* (CMS Collaboration), JHEP 04 (2017) 039.
[14] Evgeny Shulga for the ATLAS Collaboration, J. Phys.: Conf. Ser. **668**, 012078 (2016).
[15] B. Schenke, S. Schlichting, P. Tribedy, and R. Venugopalan, Phys. Rev. Lett. **117**, 162301 (2016).
[16] K. Dusling, P. Tribedy, and R. Venugopalan, Phys. Rev. D **93**, 014034 (2016).
[17] A. H. Rezaeian, Phys. Lett. B **727**, 218 (2013).
[18] G.-L. Ma and A. Bzdak, Phys. Lett. B **739**, 209 (2014).
[19] A. Bzdak and G.-L. Ma, Phys. Rev. Lett. **113**, 252301 (2014).
[20] C. Aidala *et al.* (PHENIX Collaboration), Nat. Phys. **15**, 214 (2019).
[21] S. H. Lim, J. Carlson, C. Loizides, D. Lonardoni, J. E. Lynn, J. L. Nagle, J. D. Orjuela Koop, and J. Ouellette, Phys. Rev. C **99**, 044904 (2019).
[22] Z. Citron *et al.*, CERN-LPCC-2018-07, arXiv:1812.06772.
[23] J. Schukraft, A. Timmins, and S. A. Voloshin, Phys. Lett. B **719**, 394 (2013).
[24] G. Aad *et al.* (ATLAS Collaboration), JHEP 11 (2013) 183.
[25] J. Adam *et al.* (ALICE Collaboration), Phys. Rev. C **93**, 034916 (2016).
[26] G. Aad *et al.* (ATLAS Collaboration), Phys. Rev. C **92**, 034903 (2015).
[27] A. M Sirunyan *et al.* (CMS Collaboration), Phys. Rev. C **97**, 044912 (2018).
[28] S. Acharya *et al.* (ALICE Collaboration), Phys. Lett. B **777**, 151 (2018).
[29] T. Pierog and K. Werner, Nucl. Phys. B, Proc. Suppl. **196**, 102 (2009).
[30] S. Kar *et al.*, J. Phys. G: Nucl. Part. Phys. **45**, 125103 (2018).
[31] K Werner *et al.*, J. Phys.: Conf. Ser. **535**, 012028 (2014).
[32] T. Pierog, Iu. Karpenko, J. M. Katzy, E. Yatsenko, and K. Werner, Phys. Rev. C **92**, 034906 (2015).
[33] B. Abelev *et al.* (ALICE Collaboration), Phys. Lett. B **726**, 164 (2013).
[34] J. Adam *et al.* (ALICE Collaboration), Phys. Rev. C **91**, 064905 (2015).
[35] S. Acharya *et al.* (ALICE Collaboration), JHEP 02 (2019) 150.
[36] K. Aamodt *et al.* (ALICE Collaboration), JINST **3**, S08002 (2008).
[37] B. Abelev *et al.* (ALICE Collaboration), Int. J. Mod. Phys. A **29**, 1430044 (2014).
[38] M. Cacciari, G. P. Salam, and G. Soyez, JHEP 04 (2008) 063.
[39] C. Adler *et al.* (STAR Collaboration), Phys. Rev. C **66**, 034904 (2002).
[40] S. A. Voloshin, A. M. Poskanzer, and R. Snellings, arXiv:0809.2949.
[41] E. Schnedermann, J. Sollfrank, and U. Heinz, Phys. Rev. C **48**, 2462 (1993).